

# Unconventional Thermalization of a Localized Chain Interacting with an Ergodic Bath

Konrad Pawlik,<sup>1,2,\*</sup> Nicolas Laflorencie,<sup>3,†</sup> and Jakub Zakrzewski<sup>2,4,‡</sup>

<sup>1</sup>*Szkoła Doktorska Nauk Ścisłych i Przyrodniczych, Uniwersytet Jagielloński, ulica Stanisława Łojasiewicza 11, PL-30-348 Kraków, Poland*

<sup>2</sup>*Instytut Fizyki Teoretycznej, Wydział Fizyki, Astronomii i Informatyki Stosowanej, Uniwersytet Jagielloński, ulica Stanisława Łojasiewicza 11, PL-30-348 Kraków, Poland*

<sup>3</sup>*Laboratoire de Physique Théorique, Université de Toulouse, CNRS, UPS, France*

<sup>4</sup>*Mark Kac Complex Systems Research Center, Jagiellonian University in Krakow, PL-30-348 Kraków, Poland.*

(Dated: July 25, 2025)

The study of many-body localized (MBL) phases intrinsically links spectral properties with eigenstate characteristics: localized systems exhibit Poisson level statistics and area-law entanglement entropy, while ergodic systems display volume-law entanglement and follow random matrix theory predictions, including level repulsion. Here, we introduce the interacting Anderson Quantum Sun model, which significantly deviates from these conventional expectations. In addition to standard localized and ergodic phases, we identify a regime that exhibits volume-law entanglement coexisting with intermediate spectral statistics. We also identify another non-standard regime marked by Poisson level statistics, sub-volume entanglement growth, and rare-event-dominated correlations, indicative of emerging ergodic instabilities. These results highlight unconventional routes of ergodicity breaking and offer fresh perspectives on how Anderson localization may be destabilized.

*Introduction.* Many-body localization (MBL) [1–4], a spectacular counterexample to the once dominating belief of the prevalence of ergodic dynamics in many-body interacting systems, has been extensively studied for twenty years already (see recent reviews for details [5–8]). Typically in a finite one-dimensional systems one may observe both the ergodic phase described by the eigenstate thermalization hypothesis (ETH) [9–12] for small disorder and the MBL phase with the phenomenological description provided by quasi-local integrals of motion (lioms) [13–16] for large disorder. The MBL system fails to thermalize and retains the memory of its initial state [4, 14, 17], which is accompanied by a suppression of transport [5, 18] and a slow, logarithmic in time spread of the entanglement [19–22]. The signatures of MBL were observed experimentally in relatively small systems [23–27] and at finite times, while mathematical arguments for its existence were also provided [28] (for recent advances, see also Refs. [29–31]).

This comfortable picture has been shaken [32, 33] by others who stressed a strong dependence of the ergodic-MBL crossover on the system size. In effect, the existence of the MBL phase in the thermodynamic limit remains an open question [34–50] as also summarized in a recent review [8].

Another approach, originating from the so-called avalanche scenario [51], has aimed to understand how small thermal regions (appearing, e.g., due to rare Griffiths regions of relatively weak disorder) may spread, possibly destabilizing the MBL phase. This inspired a series of effective models that emulate the influence of such thermal baths on localization [52–58]. Among those, the quantum sun (QS) model [59] distinguished itself as a toy model with remarkable properties. In particular, it was shown to exhibit an ergodicity-breaking transition with negligible finite-size effects [59] compared to paradigmatic many-body interacting models such as, e.g., the disordered Heisenberg chain, resulting in better controlled numerics. Subsequent works revealed further notable features

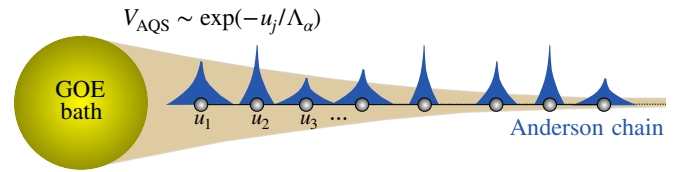


FIG. 1. Schematic of the AQS model Eq. (2). An ergodic bath is coupled to an Anderson chain via exponentially decaying interactions.

of the QS, including numerical evidence of the many-body mobility edge [60] despite earlier arguments against its existence [61], identification of Fock space localized phase, multifractal critical point across the parameter space [62] and the demonstration of the fading ergodicity ansatz [63].

*Main results.* Since the QS has proven to be a good toy model to mimic the MBL transition under the influence of an ergodic bath [51, 52, 59, 60, 63], it seems well-suited to answer one of the most fundamental questions in the field [1, 2, 64]: How can interactions with an ergodic bath destabilize an Anderson insulator, and via what mechanism(s)? To address this question, we consider the QS model, i.e., a spin chain with the interaction of individual spins to the ergodic bath decaying exponentially with the distance, enriched by  $U(1)$  nearest neighbor XY couplings; see Fig. 1 and formulae below. We refer to this construction as the Anderson Quantum Sun (AQS). Our results, summarized in the phase diagrams of Fig. 2 and Tab. I, can be outlined as follows:

- (i) For strong disorder, weak interactions with the ergodic bath turn Anderson localization into a standard MBL insulator, and sufficiently strong interactions are required to thermalize the system, as in the original QS model.
- (ii) Surprisingly, for smaller disorder, the coupling of the Anderson chain to the ergodic bath leads to an unconventional, multistage crossover toward thermalization.

(a) For weak interaction, the spectrum adheres to Poisson statistics; however, the eigenstates reveal sub-volume entanglement accompanied by unusually strong system-wide correlations dominated by rare events. This behavior contrasts sharply with a genuine many-body localized (MBL) phase, in which one would expect area-law entanglement and strictly short-range correlations.

(b) Upon increasing the coupling, before reaching the conventional ergodic thermal phase for strong enough interactions, the system enters a second anomalous regime: fully thermal (volume-law entanglement) in terms of eigenstates, but with intermediate spectral statistics. Such behavior, typical of mixed phase space dynamics [65–67], is reminiscent of features seen in integrable and delocalized quadratic models [68].

These observations support earlier theoretical predictions of an intermediate sub-volume law regime that separates the MBL and volume-law phases [69, 70]. They also shed new light on recent numerical studies reporting the existence of an intermediate regime between MBL and ETH [33, 71–76].

*The AQS model.* Our starting point is the U(1) symmetric QS model [60] (see the End Matter for details)

$$\mathcal{H}_{\text{QS}} = \mathcal{R}_{\text{QS}} + \sum_{j=1}^L \alpha^{u_j} (S_{n_j}^x S_j^x + S_{n_j}^y S_j^y) + \sum_{j=1}^L h_j S_j^z, \quad (1)$$

describing a chain of  $L$  uncoupled spins, all interacting with an ergodic bath called sun (modeled by  $N = 3$  strongly coupled spins). We aim to generalize this QS model to the AQS case, where spins in the chain are now coupled to form an Anderson chain, with the Hamiltonian:

$$\mathcal{H}_{\text{AQS}} = \mathcal{H}_{\text{QS}} + J \sum_{j=1}^{L-1} (S_j^x S_{j+1}^x + S_j^y S_{j+1}^y). \quad (2)$$

Note that, if coupling to the sun is neglected, the random magnetic field  $h_j \in [1 - W, 1 + W]$  leads to Anderson localization of the chain for any finite  $W$ , with an average many-body localization length [77] given by

$$\xi_{\text{AL}} = 1/\ln \left[ 1 + \left( \frac{W}{W_0 J} \right)^2 \right] \quad (3)$$

with  $W_0 \sim 1.2$  [78]. The interaction between the sun spins  $n_j$  and the external spins  $j$  decays with the distance  $u_j \approx j$  exponentially  $V_{\text{AQS}} = \alpha^{u_j} = \exp(-u_j/\Lambda_\alpha)$ . This defines the length scale associated with the interaction

$$\Lambda_\alpha = 1/|\ln \alpha|. \quad (4)$$

Even though the size of the sun,  $N$ , is fixed, the system can exhibit an ergodicity-breaking transition, as found in the original QS model ( $J = 0$ ) for  $\alpha^c \sim 0.75$  [59, 60], in good agreement with the prediction of the avalanche scenario  $1/\sqrt{2}$  [51, 52].

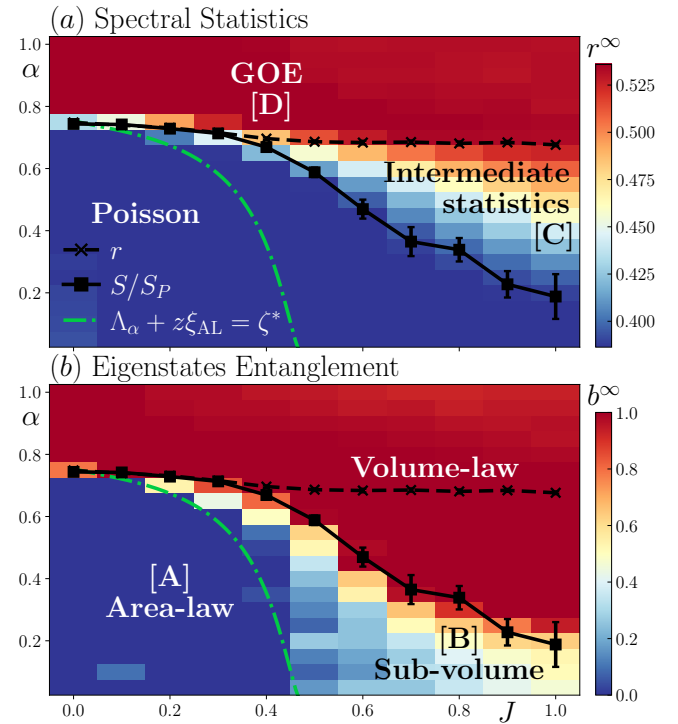


FIG. 2. Phase diagram of the AQS model. (a): gap ratio extrapolated to the thermodynamic limit  $r^\infty$ . (b): power in the power-law dependence of entropy growth  $S \propto L^b$  extrapolated to the thermodynamic limit  $b^\infty$ . Curves on both plots represent spectral (dashed black,  $\alpha_{r,\infty}^c$ ) and eigenstate (solid black,  $\alpha_{S,\infty}^c$ ) phase transition, regimes of the model are labeled with [A-D]. Dotted-dashed green analytical line signals the onset of ergodic instabilities.

The above AQS model is expected to exhibit richer behavior upon varying the free parameters  $\alpha$  and  $J$ , keeping the random-field width fixed at  $W = 0.5$ . Indeed, it involves a more realistic interplay between noninteracting localization, controlled by  $\xi_{\text{AL}}$ , and interaction with an ergodic bath governed by  $\Lambda_\alpha$ , as we discuss now in more detail, based on intensive numerics.

*Numerical methods.* We perform statistical analysis of both eigenvalues and eigenvectors. In the former case, we analyze the gap ratios  $r_i = \min(s_i, s_{i+1})/\max(s_i, s_{i+1})$  [3],

Regime	Spectrum	EE $\propto L^b$	Correlations	PE
[A]	Poisson	$b = 0$	Short range No rare events	$0 < D_q < 1$
[B]		$0 < b < 1$	Rare events	
[C]	Intermediate	$b = 1$	ETH	$D_q = 1$
[D]	GOE			

TABLE I. Properties of the different regimes of the AQS model, dashed lines corresponding to phase transitions, and labels of regimes [A-D] are the same as in Fig. 2. Participation entropy (PE) results are discussed in the End Matter.

where  $s_i = E_{i+1} - E_i$  are the energy gaps. Random matrix theory predicts [79, 80] different distributions of gap ratios for integrable and ergodic systems, with the average gap ratio,  $\langle r \rangle \approx 0.39$  for the former (corresponding to the Poisson ensemble) and  $\langle r \rangle \approx 0.53$  for generalized time-reversal invariant systems [65] corresponding to the GOE.

Regarding eigenvectors, we analyze the von Neumann entanglement entropy (EE), expressed as  $S(|\psi\rangle) = -\text{Tr}_A \rho_A \ln \rho_A$  under bipartition of the system into  $A, B$  parts, where  $\rho_A = \text{Tr}_B |\psi\rangle\langle\psi|$  is a reduced density matrix for  $A$  and  $\text{Tr}_B$  is a partial trace over  $B$ . For the  $A$  part we take the GOE sun combined with  $\lfloor (N+L)/2 \rfloor - N$  closest (with the ordering of spins dictated by the  $u_j$ ) Anderson spins. Then  $B$  is chosen as the remaining part of the system. The EE is averaged over the states corresponding to the chosen energy window. As entropy is an extensive quantity, to compare different system sizes, we introduce normalization by Page entropy  $S_P$  [81, 82], entropy of a Haar random vector from the Hilbert space, with the ratio  $S/S_P$  going from close to 0 value to 1 in the limiting cases of localized and maximally extended states, respectively.

*Vertical scans.* The results for both quantities are presented in Fig. 3 for two representative vertical scans across the  $J-\alpha$  phase diagram (Fig. 2). For small  $J = 0.2$  (left column), corresponding to short  $\xi_{AL}$ , the results strongly resemble the qualitative behavior of the U(1) QS at  $J = 0$ , with an ergodicity breaking transition observed around  $\alpha_r^c, \alpha_S^c \approx 0.75$  for both quantities  $r$  and  $S$ . This remains true for small enough

hopping  $J \leq 0.3$ , corresponding to a strong disorder in the Anderson chain, i.e.,  $W/J \gtrsim 1.7$ .

However, unexpectedly, for larger values of  $J$  (i.e., weaker disorder), for instance  $J = 0.7$  as shown in Fig. 3 (right panels), the transition points do not coincide. The entanglement transition toward ergodic behavior occurs at a significantly smaller  $\alpha_S^c$  than the gap ratio transition  $\alpha_r^c$ . Moreover, the latter transition occurs much closer to the GOE value, suggesting significant differences in the intermediate spectral statistics around the transition.

*Horizontal scan.* To gain additional insight into the discrepancy between spectral and eigenstate behaviors, we follow a horizontal cut in the phase diagram, by varying the hopping  $J$  at fixed  $\alpha = 0.35$ , see Fig. 4. By extrapolating the gap ratio  $r$  in Fig. 4(a) to the thermodynamic limit (details in [83]), we see that Poisson statistics is present only in the region of nonergodic EE, i.e. if  $S/S_P$  decreases with the system size  $L$ , see Fig. 4(b). For larger  $J$ , EE shows an ergodic behavior, with  $S/S_P \rightarrow 1$ , while the gap ratio  $r$  approaches an intermediate value between Poisson and GOE statistics. This suggests that the whole region between the critical points  $\alpha_S^c$  and  $\alpha_r^c$  (corresponding to the transition in  $S/S_P$  and  $r$ , respectively) will share this behavior, which is confirmed by the phase diagram in Fig. 2(a). A closer look at the system size dependence  $S(L)$  in Fig. 4(c) reveals that the region of nonergodic EE is divided into two distinct regimes, one showing genuine area-law entanglement [A], and an unusual extended one [B] where a sub-volume EE is observed.

To better understand these intriguing findings, we also analyze the connected correlation function of the eigenstates, following Ref. [73]:

$$C_{ij}^{\gamma\gamma} = |\langle S_i^\gamma S_j^\gamma \rangle - \langle S_i^\gamma \rangle \langle S_j^\gamma \rangle|, \quad (5)$$

with  $\gamma = x, z$ . We choose  $i = 0, 1$  (0 representing a random spin in the sun) and  $j = \lfloor L/2 \rfloor, L$ , giving 4 types of correlation with extensive  $|i - j|$ . The typical value of the connected correlation in the localized phase is expected to decay exponentially with distance  $|i - j|$  for the  $\gamma = z$  correlation, while in the ergodic phase, due to the U(1) symmetry, it follows a power-law  $\sim L^{-1}$  instead [4, 73]. Meanwhile, the  $\gamma = x$  correlation exhibits an exponential decay for both phases.

We define the typical correlation lengths  $\xi_\gamma$  of the decays

$$\overline{\ln C_{ij}^{\gamma\gamma}} = -\frac{|i - j|}{\xi_\gamma} + \mathcal{O}(1), \quad (6)$$

where  $\overline{(\cdot)}$  denotes disorder and eigenstates averaging. If  $C_{ij}^{zz}$  decays algebraically, fitting to the above form fails, and the extracted values of  $\xi_z$  will effectively grow with the system size. Taking  $\xi_x$  as the reference value, we can use  $\xi_x/\xi_z$  to detect the signatures of ergodic instabilities [73, 74], as shown in Fig. 4(d) for  $C_{1,L}$ . With increasing system size  $L$ , it would approach  $\xi_x/\xi_z \rightarrow 2$  for an Anderson model or a strongly disordered XXZ Heisenberg chain [73], which is also the behavior of the AQS for small nonzero  $J$ .

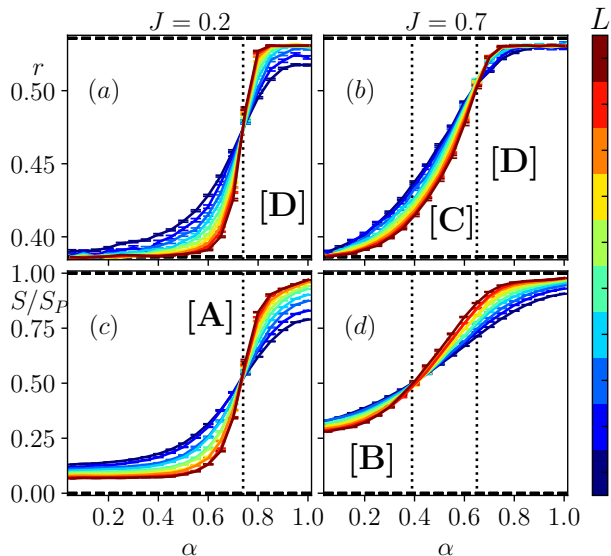


FIG. 3. High energy indicators of ergodicity-breaking, as a function of parameter  $\alpha$ , for fixed value of  $J$ . (a, b): gap ratio  $r$ . (c, d): rescaled half-chain entanglement entropy of eigenstates  $S/S_P$ . Dashed lines indicate prediction of GOE and Poisson ensemble, while dotted lines indicate prediction of Poisson ensemble. Different colors represent different system sizes - see color bar. Regimes are labeled [A-D] in accordance with Fig. 2.

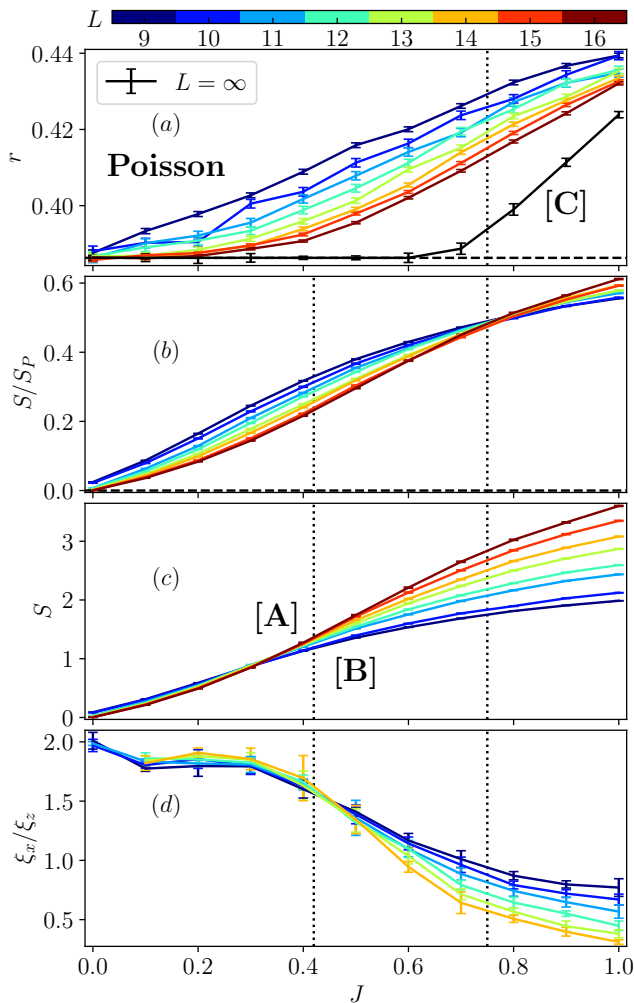


FIG. 4. Horizontal scan of the phase diagram at  $\alpha = 0.35$ . (a) Gap ratio  $r$ . (b) Rescaled entropy  $S/S_P$ . (c) Entanglement entropy  $S$ . (d) Correlation length ratio  $\xi_x/\xi_z$  of  $C_{1,L}$ , for different choices of the fitting window of system sizes  $[L-2, L+2]$ , with  $L$  indicated by the color bar. In panels (a, b), dashed horizontal lines indicate the Poisson limit, the black solid curve in (a) represents the extrapolation to the thermodynamic limit. Dotted lines indicate transitions. Data points for  $L = 12-14$  in (d) at  $J = 0$  are omitted, as they contain events with  $C_{1,L}$  below numerical precision.

Remarkably, the ergodic instabilities revealed by decreasing  $\xi_x/\xi_z$  with  $L$ , show up in the same regime [B] where sub-volume EE is observed, see Fig. 4(c), suggesting a link between the two. These results are supported by all types of correlations considered, see the End Matter. Interestingly, even at  $J = 0$ , the QS model retains a correlation length ratio  $\xi_x/\xi_z \approx 2$ .

*Phase diagram.* The two panels of Fig. 2 show the global phase diagrams from two different viewpoints: (a) spectral statistics and (b) eigenstate entanglement. In Fig. 2(a), we can see that for  $J \geq 0.4$ , a gap opens between the GOE and Poisson regimes, beyond statistical uncertainties. This indicates a new regime with volume-law entanglement and inter-

mediate statistics [C]. For smaller values of  $J$ , this extended unconventional regime shrinks and seems to merge into a critical line that ends at the QS critical point, which also exhibits intermediate statistics [60, 62]. It seems that introducing a sufficiently strong coupling  $J$  elevates the single QS critical point to a whole phase, intervening between GOE and Poisson statistics.

We now turn to the unconventional entanglement properties, illustrated by the sub-volume region [B] in Fig. 4(c). To probe the intermediate EE scaling, we fit  $S \propto L^b$  for different windows of system sizes and extrapolate the results to  $L \rightarrow \infty$ , which is depicted in Fig. 2(b). The region showing a genuine volume-law  $b = 1$  is in excellent agreement with the extrapolated eigenstate phase transition (solid curve). On the other hand, below this transition, the phase with Poisson statistics splits into two regimes: an area-law region [A] with  $b \approx 0$ , and a sub-volume regime [B] where  $0 < b < 1$ . It is worth noting that this region [B] also hosts ergodic instabilities and rare events, observed in the system-wide correlations, see the End Matter.

To better understand the crossover between [A] and [B] inside the Poisson regime, we consider the two characteristic length scales of the model: the average Anderson localization length  $\xi_{AL}$  [Eq. (3)] and the length scale  $\Lambda_\alpha$  [Eq. (4)] associated with the interaction with the sun. They clearly play different roles in the AQS model, but both control how the system gets delocalized. Increasing any of these scales clearly enhances delocalization, and if an avalanche instability exists, it could follow a generalized avalanche threshold of the form

$$\Lambda_\alpha + z\xi_{AL} = \zeta^*, \quad (7)$$

where  $z$  and  $\zeta^*$  are constants depending on the microscopic details of the model. We observe that  $z \approx 2$  and  $\zeta^* \approx 3.7$  give a good description of the crossover between [A] and [B], see the green dotted-dashed line in Fig. 2(b).

At this stage, it is important to note that the presence of the sub-volume region in the AQS model is in stark contrast to the XXZ model, where area-law entanglement entropy and Poisson level statistics always appear together [73]. The properties of all regimes are summarized in Tab. I, together with the participation entropy (PE) (for details on the PE results, see the End Matter).

*Discussion.* Our study reveals a surprising breakdown of the commonly observed correspondence between eigenstate localization and spectral statistics in many-body interacting systems. While paradigmatic models of MBL typically exhibit consistent signatures of localization in both eigenstates and level statistics, we conversely find for the interacting AQS the emergence of a volume-law entangled phase that retains intermediate level statistics in the thermodynamic limit. We also report the existence of an extended intermediate sub-volume regime associated with anomalously strong system-wide correlations that coexist with Poisson spectral statistics.

Moreover, our results for the AQS model enrich our understanding of how Anderson localization can break down due to

interactions. At small  $J/W$ , MBL is continuously connected to the Anderson insulator, similar to the behavior found in the disordered XXZ chain at large disorder [73]. However, at larger  $J/W$ , the situation differs from XXZ. Here weak interactions  $\alpha$  do not change the spectral statistics but lead to delocalized sub-volume eigenstates, between the area-law and volume-law regimes. This may be a concrete realization of the intermediate region proposed by Grover in Ref. [69]. Intriguingly, this regime also displays system-wide instabilities in correlation functions, reminiscent of the recently studied intermediate region(s) of MBL in the XXZ model [73–76].

An experimental realization of QS or AQS models remains an open challenge. One of the possibilities would be to use the flexibility of ion chains (for a review see e.g. [84]). While most of the effort with ion chains is oriented towards quantum computing [85–87], they offer an ideal medium as a quantum simulator with the ability to shape various interactions and tunnelings.

In summary, our results highlight the AQS as a promising model for studying the interplay of localization, ergodicity, and spectral statistics. They open up several avenues for future research, including the stability of the sub-volume phase, its potential connection to MBL studies, and its accessibility in current experimental platforms.

We thank A. Chandran, P. Crowley and P.R.N. Falcão for interesting discussions. We gratefully acknowledge Polish high-performance computing infrastructure PLGrid (HPC Center: ACK Cyfronet AGH) for providing computer facilities and support within computational grant no. PLG/2025/018457. This research has been funded by National Science Centre (Poland) under project 2021/43/I/ST3/01142. The study was funded by the “Research support module” as part of the “Excellence Initiative – Research University” program at the Jagiellonian University in Kraków. This study has been (partially) supported through the grant NanoX n° ANR-17-EURE-0009 in the framework of the ‘Programme des Investissements d’Avenir’. NL is supported by the ANR research grant ManyBodyNet No. ANR-24-CE30-5851, and also benefited from the support of the Fondation Simone et Cino Del Duca.

---

\* [konrad.pawlik@doctoral.uj.edu.pl](mailto:konrad.pawlik@doctoral.uj.edu.pl)

† [nicolas.laflorencie@cnsr.fr](mailto:nicolas.laflorencie@cnsr.fr)

‡ [jakub.zakrzewski@uj.edu.pl](mailto:jakub.zakrzewski@uj.edu.pl)

- [1] I. V. Gornyi, A. D. Mirlin, and D. G. Polyakov, Interacting Electrons in Disordered Wires: Anderson Localization and Low- $T$  Transport, *Phys. Rev. Lett.* **95**, 206603 (2005).
- [2] D. Basko, I. Aleiner, and B. Altshuler, Metal–insulator transition in a weakly interacting many-electron system with localized single-particle states, *Annals of Physics* **321**, 1126 (2006).
- [3] V. Oganesyan and D. A. Huse, Localization of interacting fermions at high temperature, *Phys. Rev. B* **75**, 155111 (2007).
- [4] A. Pal and D. A. Huse, Many-body localization phase transition, *Phys. Rev. B* **82**, 174411 (2010).
- [5] R. Nandkishore and D. A. Huse, Many-Body Localization and Thermalization in Quantum Statistical Mechanics, *Annual Review of Condensed Matter Physics* **6**, 15 (2015).
- [6] F. Alet and N. Laflorencie, Many-body localization: An introduction and selected topics, *Comptes Rendus Physique* **19**, 498 (2018).
- [7] D. A. Abanin, E. Altman, I. Bloch, and M. Serbyn, Colloquium: Many-body localization, thermalization, and entanglement, *Rev. Mod. Phys.* **91**, 021001 (2019).
- [8] P. Sierant, M. Lewenstein, A. Scardicchio, L. Vidmar, and J. Zakrzewski, Many-body localization in the age of classical computing, *Reports on Progress in Physics* **88**, 026502 (2025).
- [9] J. M. Deutsch, Quantum statistical mechanics in a closed system, *Phys. Rev. A* **43**, 2046 (1991).
- [10] M. Srednicki, Chaos and quantum thermalization, *Phys. Rev. E* **50**, 888 (1994).
- [11] M. Rigol, V. Dunjko, and M. Olshanii, Thermalization and its mechanism for generic isolated quantum systems, *Nature* **452**, 854 EP (2008).
- [12] L. D’Alessio, Y. Kafri, A. Polkovnikov, and M. Rigol, From quantum chaos and eigenstate thermalization to statistical mechanics and thermodynamics, *Advances in Physics* **65**, 239 (2016).
- [13] M. Serbyn, Z. Papić, and D. A. Abanin, Local conservation laws and the structure of the many-body localized states, *Phys. Rev. Lett.* **111**, 127201 (2013).
- [14] D. A. Huse, R. Nandkishore, and V. Oganesyan, Phenomenology of fully many-body-localized systems, *Phys. Rev. B* **90**, 174202 (2014).
- [15] V. Ros, M. Mueller, and A. Scardicchio, Integrals of motion in the many-body localized phase, *Nuclear Physics B* **891**, 420 (2015).
- [16] S. J. Thomson and M. Schiró, Time evolution of many-body localized systems with the flow equation approach, *Phys. Rev. B* **97**, 060201 (2018).
- [17] D. J. Luitz, N. Laflorencie, and F. Alet, Many-body localization edge in the random-field Heisenberg chain, *Phys. Rev. B* **91**, 081103 (2015).
- [18] M. Žnidarič, A. Scardicchio, and V. K. Varma, Diffusive and subdiffusive spin transport in the ergodic phase of a many-body localizable system, *Phys. Rev. Lett.* **117**, 040601 (2016).
- [19] G. D. Chiara, S. Montangero, P. Calabrese, and R. Fazio, Entanglement entropy dynamics of heisenberg chains, *Journal of Statistical Mechanics: Theory and Experiment* **2006**, P03001 (2006).
- [20] M. Žnidarič, T. Prosen, and P. Prelovšek, Many-body localization in the Heisenberg XXZ magnet in a random field, *Phys. Rev. B* **77**, 064426 (2008).
- [21] J. H. Bardarson, F. Pollmann, and J. E. Moore, Unbounded growth of entanglement in models of many-body localization, *Phys. Rev. Lett.* **109**, 017202 (2012).
- [22] M. Serbyn, Z. Papić, and D. A. Abanin, Universal slow growth of entanglement in interacting strongly disordered systems, *Phys. Rev. Lett.* **110**, 260601 (2013).
- [23] M. Schreiber, S. S. Hodgman, P. Bordia, H. P. Lüschen, M. H. Fischer, R. Vosk, E. Altman, U. Schneider, and I. Bloch, Observation of many-body localization of interacting fermions in a quasirandom optical lattice, *Science* **349**, 842 (2015).
- [24] P. Bordia, H. P. Lüschen, S. S. Hodgman, M. Schreiber, I. Bloch, and U. Schneider, Coupling identical one-dimensional many-body localized systems, *Phys. Rev. Lett.* **116**, 140401 (2016).
- [25] J. Smith, A. Lee, P. Richerme, B. Neyenhuis, P. W. Hess, P. Hauke, M. Heyl, D. A. Huse, and C. Monroe, Many-body localization in a quantum simulator with programmable random

- disorder, *Nature Physics* **12**, 907 (2016).
- [26] H. P. Lüschen, P. Bordia, S. Scherg, F. Alet, E. Altman, U. Schneider, and I. Bloch, Observation of slow dynamics near the many-body localization transition in one-dimensional quasiperiodic systems, *Phys. Rev. Lett.* **119**, 260401 (2017).
- [27] J. Léonard, S. Kim, M. Rispoli, A. Lukin, R. Schittko, J. Kwan, E. Demler, D. Sels, and M. Greiner, Probing the onset of quantum avalanches in a many-body localized system, *Nature Physics* **19**, 481 (2023).
- [28] J. Z. Imbrie, Diagonalization and many-body localization for a disordered quantum spin chain, *Phys. Rev. Lett.* **117**, 027201 (2016).
- [29] C. Yin, R. Nandkishore, and A. Lucas, Eigenstate localization in a many-body quantum system, *Phys. Rev. Lett.* **133**, 137101 (2024).
- [30] W. D. Roeck, L. Giacomin, F. Huveneers, and O. Prosniak, Absence of normal heat conduction in strongly disordered interacting quantum chains (2024), arXiv:2408.04338 [math-ph].
- [31] C. L. Baldwin, Subballistic operator growth in spin chains with heavy-tailed random fields, *Phys. Rev. B* **111**, 184204 (2025).
- [32] J. Šuntajs, J. Bonča, T. Prosen, and L. Vidmar, Quantum chaos challenges many-body localization, *Phys. Rev. E* **102**, 062144 (2020).
- [33] F. Weiner, F. Evers, and S. Bera, Slow dynamics and strong finite-size effects in many-body localization with random and quasiperiodic potentials, *Phys. Rev. B* **100**, 104204 (2019).
- [34] P. Sierant, D. Delande, and J. Zakrzewski, Thouless time analysis of anderson and many-body localization transitions, *Phys. Rev. Lett.* **124**, 186601 (2020).
- [35] R. K. Panda, A. Scardicchio, M. Schulz, S. R. Taylor, and M. Žnidarič, Can we study the many-body localisation transition?, *Europhysics Letters* **128**, 67003 (2020).
- [36] D. Sels and A. Polkovnikov, Dynamical obstruction to localization in a disordered spin chain, *Phys. Rev. E* **104**, 054105 (2021).
- [37] M. Kiefer-Emmanouilidis, R. Unanyan, M. Fleischhauer, and J. Sirker, Evidence for unbounded growth of the number entropy in many-body localized phases, *Phys. Rev. Lett.* **124**, 243601 (2020).
- [38] P. Sierant, M. Lewenstein, and J. Zakrzewski, Polynomially filtered exact diagonalization approach to many-body localization, *Phys. Rev. Lett.* **125**, 156601 (2020).
- [39] D. Abanin, J. Bardarson, G. D. Tomasi, S. Gopalakrishnan, V. Khemani, S. Parameswaran, F. Pollmann, A. Potter, M. Serbyn, and R. Vasseur, Distinguishing localization from chaos: Challenges in finite-size systems, *Annals of Physics* **427**, 168415 (2021).
- [40] M. Kiefer-Emmanouilidis, R. Unanyan, M. Fleischhauer, and J. Sirker, Unlimited growth of particle fluctuations in many-body localized phases, *Annals of Physics* **435**, 168481 (2021), special Issue on Localisation 2020.
- [41] R. Ghosh and M. Žnidarič, Resonance-induced growth of number entropy in strongly disordered systems, *Phys. Rev. B* **105**, 144203 (2022).
- [42] D. Sels, Bath-induced delocalization in interacting disordered spin chains, *Phys. Rev. B* **106**, L020202 (2022).
- [43] P. Sierant and J. Zakrzewski, Challenges to observation of many-body localization, *Phys. Rev. B* **105**, 224203 (2022).
- [44] D. Sels and A. Polkovnikov, Thermalization of dilute impurities in one-dimensional spin chains, *Phys. Rev. X* **13**, 011041 (2023).
- [45] A. Morningstar, L. Colmenarez, V. Khemani, D. J. Luitz, and D. A. Huse, Avalanches and many-body resonances in many-body localized systems, *Phys. Rev. B* **105**, 174205 (2022).
- [46] N. Laflorencie, G. Lemarié, and N. Macé, Chain breaking and Kosterlitz-Thouless scaling at the many-body localization transition in the random-field Heisenberg spin chain, *Phys. Rev. Research* **2**, 042033 (2020).
- [47] J. Šuntajs, J. Bonča, T. Prosen, and L. Vidmar, Ergodicity breaking transition in finite disordered spin chains, *Phys. Rev. B* **102**, 064207 (2020).
- [48] D. J. Luitz and Y. B. Lev, Absence of slow particle transport in the many-body localized phase, *Phys. Rev. B* **102**, 100202 (2020).
- [49] P. Sierant, M. Lewenstein, A. Scardicchio, and J. Zakrzewski, Stability of many-body localization in floquet systems, *Phys. Rev. B* **107**, 115132 (2023).
- [50] T. Szodra, P. Sierant, M. Lewenstein, and J. Zakrzewski, Tracking locality in the time evolution of disordered systems, *Phys. Rev. B* **107**, 054204 (2023).
- [51] W. De Roeck and F. Huveneers, Stability and instability towards delocalization in many-body localization systems, *Phys. Rev. B* **95**, 155129 (2017).
- [52] D. J. Luitz, F. Huveneers, and W. De Roeck, How a small quantum bath can thermalize long localized chains, *Phys. Rev. Lett.* **119**, 150602 (2017).
- [53] I.-D. Potirniche, S. Banerjee, and E. Altman, Exploration of the stability of many-body localization in  $d > 1$ , *Phys. Rev. B* **99**, 205149 (2019).
- [54] P. J. D. Crowley and A. Chandran, Avalanche induced coexisting localized and thermal regions in disordered chains, *Phys. Rev. Res.* **2**, 033262 (2020).
- [55] P. J. D. Crowley and A. Chandran, Mean-field theory of failed thermalizing avalanches, *Phys. Rev. B* **106**, 184208 (2022).
- [56] T. Szodra, P. Sierant, M. Lewenstein, and J. Zakrzewski, Catching thermal avalanches in the disordered xxz model, *Phys. Rev. B* **109**, 134202 (2024).
- [57] L. Colmenarez, D. J. Luitz, and W. De Roeck, Ergodic inclusions in many-body localized systems, *Phys. Rev. B* **109**, L081117 (2024).
- [58] V. Berger, A. Nava, J. H. Bardarson, and C. Artiago, Numerical study of disordered noninteracting chains coupled to a local lindblad bath (2024), arXiv:2412.03233 [cond-mat.dis-nn].
- [59] J. Šuntajs and L. Vidmar, Ergodicity breaking transition in zero dimensions, *Phys. Rev. Lett.* **129**, 060602 (2022).
- [60] K. Pawlik, P. Sierant, L. Vidmar, and J. Zakrzewski, Many-body mobility edge in quantum sun models, *Phys. Rev. B* **109**, L180201 (2024).
- [61] W. De Roeck, F. Huveneers, M. Müller, and M. Schiulaz, Absence of many-body mobility edges, *Phys. Rev. B* **93**, 014203 (2016).
- [62] J. Šuntajs, M. Hopjan, W. De Roeck, and L. Vidmar, Similarity between a many-body quantum avalanche model and the ultrametric random matrix model, *Phys. Rev. Res.* **6**, 023030 (2024).
- [63] R. Świątek, P. Łydzba, and L. Vidmar, Fading ergodicity meets maximal chaos, *Phys. Rev. B* **111**, 184203 (2025).
- [64] L. Fleishman and P. W. Anderson, Interactions and the Anderson transition, *Phys. Rev. B* **21**, 2366 (1980).
- [65] F. Haake, *Quantum Signatures of Chaos* (Springer, Berlin, 2010).
- [66] M. Serbyn and J. E. Moore, Spectral statistics across the many-body localization transition, *Phys. Rev. B* **93**, 041424 (2016).
- [67] P. Sierant and J. Zakrzewski, Level statistics across the many-body localization transition, *Phys. Rev. B* **99**, 104205 (2019).
- [68] P. Łydzba, R. Świątek, M. Mierzejewski, M. Rigol, and L. Vidmar, Normal weak eigenstate thermalization, *Phys. Rev. B* **110**, 104202 (2024).
- [69] T. Grover, Certain general constraints on the many-body local-

- ization transition (2014), arXiv:1405.1471 [cond-mat.dis-nn].
- [70] C. Monthus, Many-body-localization transition: strong multifractality spectrum for matrix elements of local operators, *Journal of Statistical Mechanics: Theory and Experiment* **2016**, 073301 (2016).
- [71] P. T. Dumitrescu, A. Goremykina, S. A. Parameswaran, M. Serbyn, and R. Vasseur, Kosterlitz-thouless scaling at many-body localization phase transitions, *Phys. Rev. B* **99**, 094205 (2019).
- [72] F. Evers, I. Modak, and S. Bera, Internal clock of many-body delocalization, *Phys. Rev. B* **108**, 134204 (2023).
- [73] J. Colbois, F. Alet, and N. Laflorencie, Interaction-driven instabilities in the random-field  $xxz$  chain, *Phys. Rev. Lett.* **133**, 116502 (2024).
- [74] J. Colbois, F. Alet, and N. Laflorencie, Statistics of systemwide correlations in the random-field  $xxz$  chain: Importance of rare events in the many-body localized phase, *Phys. Rev. B* **110**, 214210 (2024).
- [75] G. Biroli, A. K. Hartmann, and M. Tarzia, Large-deviation analysis of rare resonances for the many-body localization transition, *Phys. Rev. B* **110**, 014205 (2024).
- [76] N. Laflorencie, J. Colbois, and F. Alet, *Cat states carrying long-range correlations in the many-body localized phase* (2025), arXiv:2504.10566 [cond-mat.dis-nn].
- [77] The phenomenological expression Eq. (3) yields an average localization length, averaged over the density of single-particle states, see Ref. [88].
- [78] As noted in Ref. [88],  $W_0$  slightly varies with  $W/J$ , from 1.13 at strong disorder to 1.22 at weak disorder.
- [79] Y. Y. Atas, E. Bogomolny, O. Giraud, and G. Roux, Distribution of the ratio of consecutive level spacings in random matrix ensembles, *Phys. Rev. Lett.* **110**, 084101 (2013).
- [80] O. Giraud, N. Macé, E. Vernier, and F. Alet, Probing symmetries of quantum many-body systems through gap ratio statistics, *Phys. Rev. X* **12**, 011006 (2022).
- [81] D. N. Page, Average entropy of a subsystem, *Phys. Rev. Lett.* **71**, 1291 (1993).
- [82] E. Bianchi, L. Hackl, M. Kieburg, M. Rigol, and L. Vidmar, Volume-Law Entanglement Entropy of Typical Pure Quantum States, *PRX Quantum* **3**, 030201 (2022).
- [83] See Supplementary Material at [URL will be inserted by publisher] for details on calculation of spectral form factor, Thouless time, scaling of critical points and discussion of statistical uncertainties. It contains references [38, 49, 89–91].
- [84] R. Blatt and C. F. Roos, Quantum simulations with trapped ions, *Nature Physics* **8**, 277 (2012).
- [85] J. I. Cirac and P. Zoller, Quantum computations with cold trapped ions, *Phys. Rev. Lett.* **74**, 4091 (1995).
- [86] J. I. Cirac and P. Zoller, A scalable quantum computer with ions in an array of microtraps, *Nature* **404**, 579 (2000).
- [87] C. D. Bruzewicz, J. Chiaverini, R. McConnell, and J. M. Sage, Trapped-ion quantum computing: Progress and challenges, *Applied Physics Reviews* **6**, 021314 (2019).
- [88] J. Colbois and N. Laflorencie, Breaking the chains: Extreme value statistics and localization in random spin chains, *Phys. Rev. B* **108**, 144206 (2023).
- [89] E. J. Torres-Herrera, G. De Tomasi, M. Schiulaz, F. Pérez-Bernal, and L. F. Santos, Self-averaging in many-body quantum systems out of equilibrium: Approach to the localized phase, *Phys. Rev. B* **102**, 094310 (2020).
- [90] M. Schiulaz, E. J. Torres-Herrera, F. Pérez-Bernal, and L. F. Santos, Self-averaging in many-body quantum systems out of equilibrium: Chaotic systems, *Phys. Rev. B* **101**, 174312 (2020).
- [91] G. Cowan, *Statistical data analysis* (Oxford University Press, USA, 1998).
- [92] N. Macé, F. Alet, and N. Laflorencie, Multifractal scalings across the many-body localization transition, *Phys. Rev. Lett.* **123**, 180601 (2019).

## End Matter

### The U(1) symmetric quantum sun model

The construction of the U(1) symmetric QS model [60], described by Eq. (1), is briefly summarized. This spin-1/2 model consists of two subsystems:  $N = 3$  spins internally described by a random  $2^N \times 2^N$  matrix  $R_{QS}$  from the Gaussian Orthogonal Ensemble (GOE) acting as a thermal bath for the rest of the system. Here  $R_{QS} = \frac{\beta}{2}(B + B^T)$ , with fixed  $\beta = 0.3$  and matrix elements  $B_{ij}$  given by i.i.d. standard Gaussian distributions. Furthermore, all matrix elements  $(R_{QS})_{ij}$  that spoil commutation with the U(1) symmetry generator  $\hat{S}_{\text{tot}}^z = \sum_{j=1-N}^L \hat{S}_j^z$  are fixed as 0. The second component of the model is the localized chain of  $L \gg N$  spins that do not interact with each other. A random magnetic field  $h_j \in [1 - W, 1 + W]$  acts at each spin outside the sun, where the disorder strength is fixed as  $W = 1/2$ . The interaction between both parts exponentially decreases with the distance  $u_j$  between the localized spin and the randomly chosen spin of the sun  $n_j$  as  $V_{AQS} = \alpha^{u_j} = \exp(-u_j/\Lambda_\alpha)$ . Moreover, positional disorder  $u_j \in [j - \zeta, j + \zeta]$  with  $\zeta = 0.2$  is introduced. Its role is purely numerical, as it helps to reduce the number

of disorder realizations required for a good convergence of the results.

### Numerical details

Our analysis is restricted to the largest symmetry sector of the model, namely  $S_{\text{tot}}^z = 0$  for even  $N + L$ , and  $S_{\text{tot}}^z = -1/2$  otherwise. For small system sizes,  $N + L \leq 13$ , we perform full exact diagonalization of Eq. (2) while for larger systems  $13 < N + L \leq 20$  the POLFED algorithm [38] is used. We take into consideration the eigenenergies in the largest density of states window  $\varepsilon \in [0.5 - \varepsilon_0, 0.5 + \varepsilon_0]$  (but not less than 30 energies), with  $\varepsilon = \frac{E - E_{\text{min}}}{E_{\text{max}} - E_{\text{min}}} \in [0, 1]$  and  $\varepsilon_0 = 0.005$ . Those are disorder averaged with  $10^4$  realizations for  $L = 7$ , with  $3 \cdot 10^3$  for  $7 < L < 16$  and  $10^3$  realizations for larger systems.

A more quantitative study of phase transitions is possible using a standard approach [38, 49] of estimating the critical point at finite size  $\alpha_{r,L}^c$  and  $\alpha_{s,L}^c$ . Utilizing consistent scaling of this value with system size  $L$  we are able to extrapolate the

results to  $L \rightarrow \infty$ , obtaining the phase boundary  $\alpha_{r,\infty}^c$  and  $\alpha_{S,\infty}^c$  [83].

### Multifractal analysis

To complement the study of eigenstates  $|\psi\rangle$ , we consider the participation entropy (PE)  $P_q$  [92]

$$|\psi\rangle = \sum_{\alpha=1}^{\mathcal{D}} \psi_{\alpha} |\alpha\rangle, \quad P_q = \frac{1}{1-q} \ln \left[ \sum_{\alpha=1}^{\mathcal{D}} |\psi_{\alpha}|^{2q} \right], \quad (8)$$

where  $\mathcal{D}$  is the Hilbert space dimension, and  $|\alpha\rangle$  denotes a spin product state. In the limit  $q \rightarrow 1$ , one obtains the Shannon participation entropy

$$P_1 = - \sum_{\alpha} |\psi_{\alpha}|^2 \ln |\psi_{\alpha}|^2. \quad (9)$$

This quantity captures how the state spreads over the computational basis, with limiting behaviors  $P_q = \text{const}$  for a Fock-space localized system and  $P_q = \ln \mathcal{D}$  for a fully ergodic one. Intermediate multifractal behavior is described by

$$P_q = D_q \ln \mathcal{D} + b_q, \quad (10)$$

which also encompasses both the limiting cases for  $D_q = 0$  and  $D_q = 1$ . Following a procedure analogous to that used for entanglement entropy in Fig. 2(b), we obtain Fig. 5 from the scaling analysis of  $P_q$ .

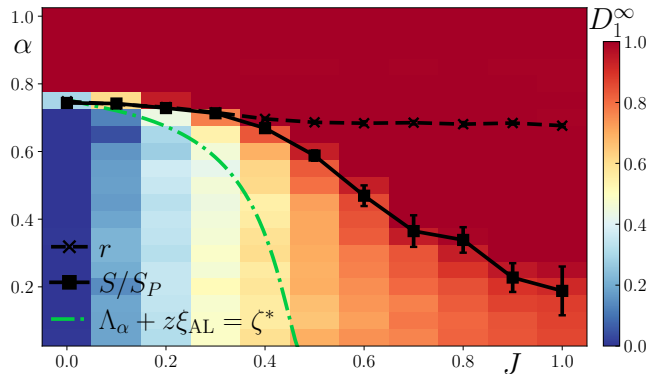


FIG. 5. Multifractal dimension  $D_1$  of eigenstates in the AQS model. For explanations of the lines, see Fig. 2 of the main text.

It is evident that the region of volume-law entanglement entropy aligns perfectly with  $D_1 = 1$ , suggesting fully ergodic eigenstates in that regime. By contrast, the area-law [A] and sub-volume [B] regimes on the phase diagram (Fig. 2) are characterized by the fractal dimension inherited from the Anderson chain, corresponding to  $\alpha = 0$ . The Fock-space localization is observed only in the QS model ( $J = 0$ ), consistent with Ref. [62].

### Ergodic instability in correlation functions

#### Correlation length ratios

The regime [B] of sub-volume entanglement growth (see Fig. 2 for the labeling of regions) exhibits ergodic characteristics in correlation functions, evidenced by a decreasing correlation length ratio  $\xi_x/\xi_z$  with increasing system size  $L$  in the fit  $[L-2, L+2]$ , as shown in Fig. 4(d) for the correlation  $C_{1,L}$ . This trend is robust for any correlation over an extensive distance  $|i-j|$ ; in Fig. 6, we demonstrate it for  $i=0, 1$  (with 0 representing a random spin from the sun) and  $j = \lfloor L/2 \rfloor, L$ . We note that the correlations with  $j = \lfloor L/2 \rfloor$  behave slightly differently for even and odd system sizes  $L$ , thus the fit to extract the correlation length  $\xi_x, \xi_z$  is performed for  $\{L-2, L, L+2\}$ , without mixing system sizes of different parity. In addition to marking the spectral (black dashed line) and eigenstate (black solid line) transitions, we also indicate the onset of ergodic instability with a black dotted line. For each  $J$ , this line corresponds to the smallest value of  $\alpha$  at which a statistically significant decrease in  $\xi_x/\xi_z$  is observed.

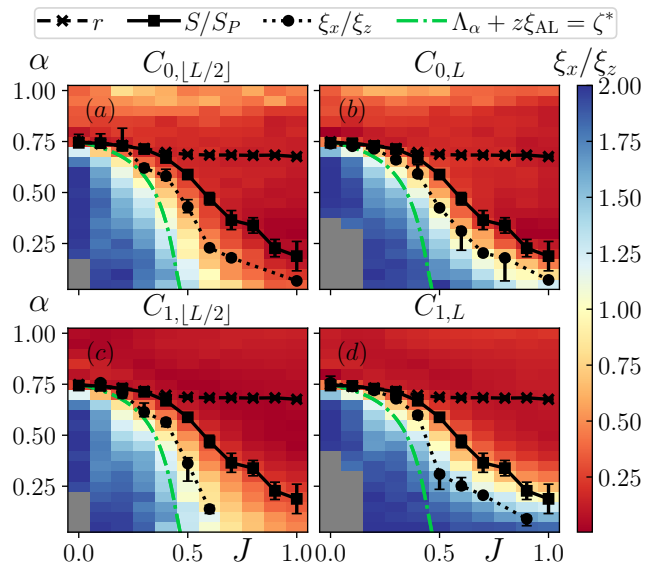


FIG. 6. Phase diagram of AQS model in terms of correlation length ratios  $\xi_x/\xi_z$ , type of the correlation indicated above each panel. Spectral ( $r$ ) and entanglement entropy ( $S/S_P$ ) transitions are the same as in Fig. 2. The  $\xi_x/\xi_z$  dotted line marks the onset of ergodic instability, with the smallest alpha that has noticeable decrease of this ratio with system size  $L$ . Color map corresponds to a fit over the system sizes  $L \in [12, 16]$ . Points on the phase diagram where correlations in some states fell below numerical precision are excluded and shown in gray.

### Rare events of large system-wide correlations

To investigate rare events involving system-wide correlations, we introduce a rescaled correlation quantity,  $\ell_{ij}^{\gamma\gamma}$

$$\ell_{ij}^{\gamma\gamma} = -\ln |4C_{ij}^{\gamma\gamma}|, \quad (11)$$

with  $\gamma = x, z$ . This transformation expands the region corresponding to large correlations,  $|C_{ij}^{\gamma\gamma}| \approx 1/4$ , mapping them to small values of rescaled correlation, while weak correlations yield large  $\ell_{ij}^{\gamma\gamma}$ . The numerical histograms for  $\ell_{0, \lfloor L/2 \rfloor}^{zz}$  are shown in Fig. 7, where all regimes [A-D] from the phase diagram of the AQS model (Fig. 2) are analyzed. In the strongly localized regime [A] (Fig. 7(a)), the number of large correlation events exponentially decreases with the system size  $L$ , similarly to the behavior in the deep MBL regime of the XXZ model [74]. In contrast, the region [B] (Fig. 7(b)), which exhibits ergodic instability in correlation functions, shows a power-law tail at small values of  $\ell$ , involving a significant fraction of all eigenstates. This feature resembles the recently proposed intermediate region between the MBL and ergodic phases of the XXZ model [74, 76]. Meanwhile, regions [C] and [D] (Fig. 7(c, d)) show a rapid suppression of such large-correlation events with system size, consistent with expectations for random eigenstates obeying ETH.

Based on the observed ergodic instabilities and rare events, two possible scenarios arise for the sub-volume region [B]: thermal avalanches may ultimately drive it towards ergodicity with volume-law entanglement growth, or, alternatively, these effects may remain insufficient, consistent with our EE results, leaving the region nonergodic.

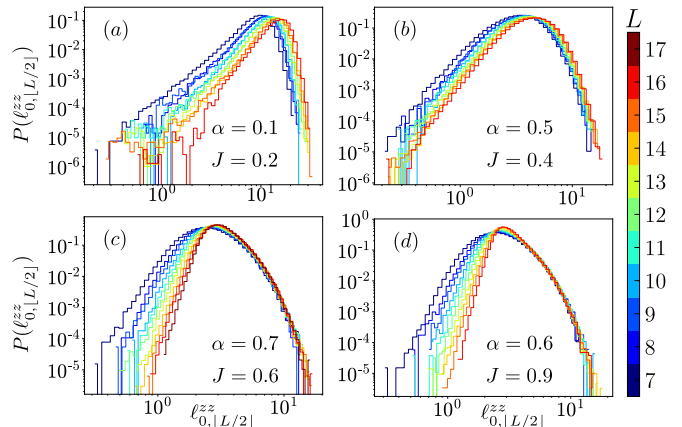


FIG. 7. Histograms of rescaled correlation function  $\ell_{0, \lfloor L/2 \rfloor}^{zz}$  for eigenstates of the AQS model. Panels (a-d) correspond to representative  $\alpha, J$  points from regime [A-D], respectively. System size is indicated by the color map.

### Supplementary material for Unconventional Thermalization of a Localized Chain Interacting with an Ergodic Bath

#### Statistical uncertainties

In the analysis of the main text, we considered an observable  $O$  averaged over an energy window, but such single disorder realization averages  $O_S$  are known not to be self-averaging in some systems [89, 90], which means that its variance  $\langle (O_S - \langle O_S \rangle)^2 \rangle$ , where  $\langle \cdot \rangle$  means average over disorder realizations, may not decrease with increasing system size. Instead, one needs to consider quantities averaged over disorder realizations  $\langle O_S \rangle$ , which is denoted  $\langle O \rangle$  for short. As we consider uncorrelated realizations, we may compute the standard deviation of such an average as [49]:

$$\sigma_O = \frac{\langle (O_S - \langle O \rangle)^2 \rangle^{1/2}}{N_{\text{dis}}^{1/2}}, \quad (S.1)$$

where  $N_{\text{dis}}$  is the number of disorder realizations used for the calculation of  $\langle O \rangle$ .

The estimate of the critical point is obtained using two distinct methods, described in detail in Sec. **Extraction and scaling of the critical point**. Due to a different character of these methods, the corresponding uncertainties are computed differently.

For the method based on crossings of numerical curves, we consider two single-parameter functions  $f_1(\alpha)$  and  $f_2(\alpha)$  with pointwise uncertainties  $\sigma_1(\alpha)$  and  $\sigma_2(\alpha)$ . The function  $\chi^2(\alpha)$  is defined:

$$\chi_L^2(\alpha) = \frac{[f_1(\alpha) - f_2(\alpha)]^2}{\sigma_1^2(\alpha) + \sigma_2^2(\alpha)}. \quad (S.2)$$

The zeros of the function  $\chi^2(\alpha_0)$  correspond to intersection points  $\alpha_0$  of the two functions. Near such a point,  $\chi^2(\alpha)$  exhibits a quadratic minimum. If the curves are well separated away from the crossing (i.e., not approximately parallel), the equation  $\chi^2(\alpha) = 1$  has two solutions  $\alpha_- < \alpha_+$ . The quantity  $(\alpha_+ - \alpha_-)/2$  has a statistical interpretation of the uncertainty of  $\alpha_0$  [91]. The standard uncertainty propagation is then used to estimate the uncertainty of the function value at the crossing,  $f_1(\alpha_0) = f_2(\alpha_0)$ .

The second method determines the critical point by locating where a curve reaches a fixed threshold value. Here, the uncertainty is estimated via bootstrapping: we repeat the extraction procedure 1000 times, each time by sampling data points from

normal distributions with mean  $f(\alpha)$  and standard deviation  $\sigma(\alpha)$ . The standard deviation of the resulting set of critical point estimates is taken as the uncertainty of the critical point.

### Extraction and scaling of the critical point

To estimate the critical point of the model in the thermodynamic limit, a measure of the critical point for finite system sizes  $L$  must be introduced, and then these results must be extrapolated  $L \rightarrow \infty$ . We employ two definitions of the critical point, the first based on crossing of the finite-size curves, the other using a threshold value near GOE.

For the crossing method, let  $f_1(\alpha)$  be a numerical curve for  $J$ , the system size  $L - 1$ , and the given observable ( $r$  or entropy), then  $f_2(\alpha)$  is an analogous curve for  $L + 1$ . Furthermore, let  $\sigma_1, \sigma_2$  be the corresponding uncertainties. We can define  $\alpha_L^{c, \text{cross}}$  as their crossing point  $\alpha_0$  with its standard deviation  $(\alpha_+ - \alpha_-)/2$ , following the notation of the Sec. **Statistical uncertainties**. To obtain the intersection numerically, we first visually estimate  $\alpha'_0$  where it is expected, and then interpolate  $f_1$  and  $f_2$  with polynomials of degree 3 in a range  $[\alpha'_0 - 0.04, \alpha'_0 + 0.04]$ . The small interpolation range eliminates accidental crossings. Example extractions are shown in Fig. S.1

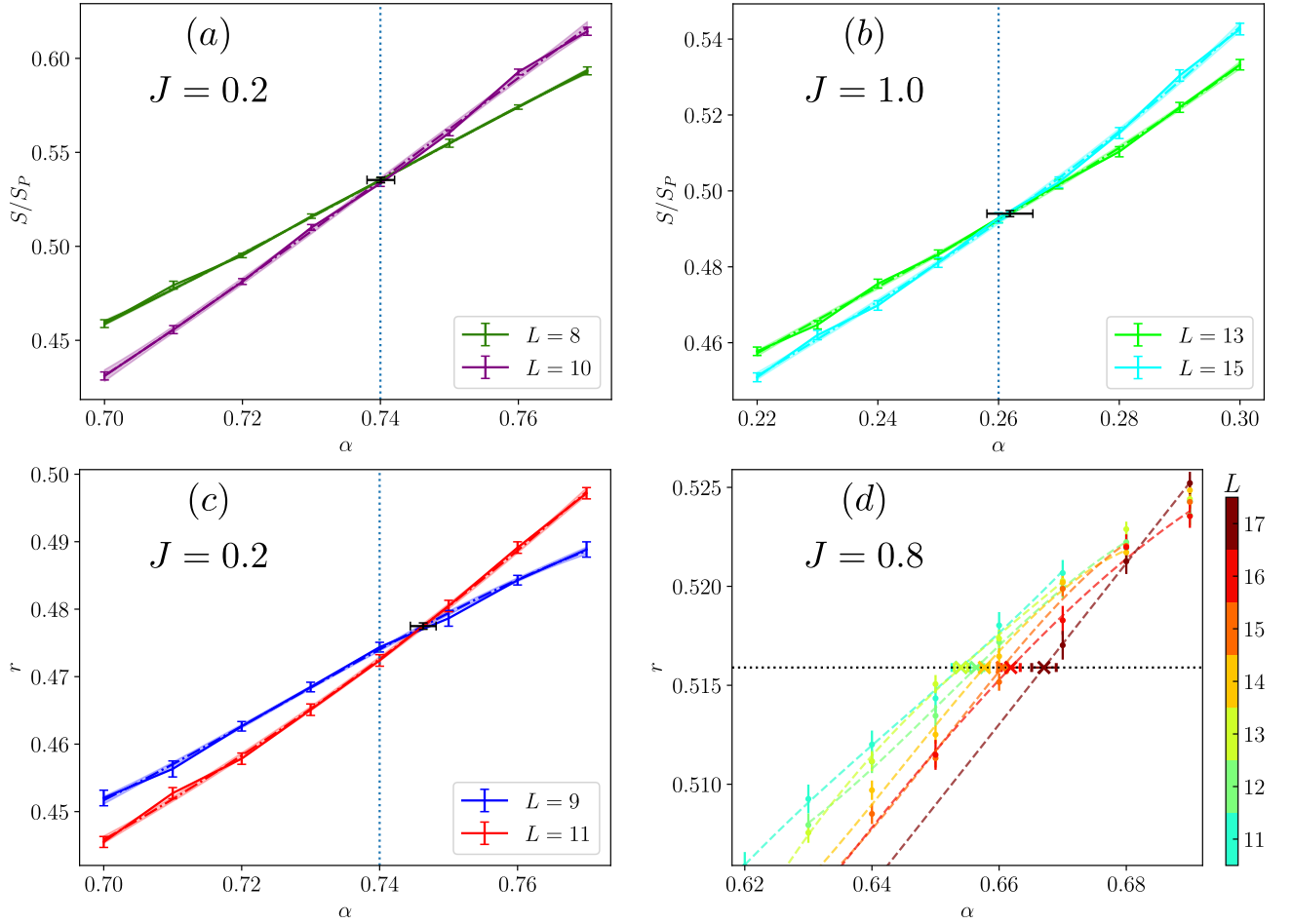


FIG. S.1. Extraction of the critical point. Crossing method: curves corresponding to system sizes  $L - 1$  and  $L + 1$  for (a, b): rescaled entanglement entropy  $S/S_P$  and (c): gap ratio  $r$ . A dotted vertical line corresponds to visual estimate  $\alpha'_0$ , while black error bars give uncertainties for the coordinates of the crossing point. Threshold method (d): numerical curves and polynomial fits used for the extraction. Horizontal dotted line indicates  $f_{\text{thresh}} = 0.02$ , crosses show obtained values of the critical point together with uncertainty.

In the threshold method, we again take numerical curves  $f(\alpha)$ , which correspond to either the gap ratio  $r$  or the entropy  $S/S_P$ , and then extract  $\alpha_L^{c, \text{thresh}}$  such that

$$f(\alpha_L^{c, \text{thresh}}) = f_{\text{GOE}} - f_{\text{thresh}}. \quad (\text{S.3})$$

In extraction of  $\alpha_L^{c,\text{thresh}}$ , we fitted the numerical data  $f(\alpha)$  with a polynomial of degree 3 in a small window of  $\alpha$  near the GOE value  $f_{\text{GOE}}$ , avoiding the region where  $f(\alpha)$  saturates on the value  $f_{\text{GOE}}$ . The example of this procedure is presented in Fig. S.1(d).

For the eigenstate data,  $S/S_P$ , the crossing method is more reliable, as the curves intersect well away from the limiting values. We note that the threshold method for relatively large  $f_{\text{thresh}} = 0.4$  yields nearly identical estimates of the transition at the thermodynamic limit  $\alpha_\infty^c$ . In contrast, for the spectral gap ratio  $r$ , the crossing method is optimal only for small coupling  $J \leq 0.2$ ; at larger  $J$ , the crossings occur too close to the GOE value  $r_{\text{GOE}}$ , making the threshold method more suitable. For  $J \geq 0.3$ , we adopt  $f_{\text{thresh}} = 0.02$ , although other values do not result in any qualitative changes. In applying the threshold method, we consider only system sizes  $L > 10$  to mitigate finite-size effects. The critical point determined using the preferred method in each case is denoted as  $\alpha_L^c$ .

The finite-size estimation of the critical point  $\alpha_L^c$  follows a system size dependence:

$$\alpha_L^c = a/L + \alpha_\infty^c, \quad (\text{S.4})$$

which enables extrapolation of the critical point to the thermodynamic limit [38, 49], see Fig. S.2. For the gap ratio  $r$ , the crossings  $\alpha_L^{c,\text{cross}}$  (Fig. S.2(a) for  $J \leq 0.2$ ) follow a finite-size scaling different from  $\alpha_L^{c,\text{thresh}}$  (Fig. S.2(a) for  $J \geq 0.3$ ), the former trying to directly estimate the critical point, while the latter serves as the upper bound instead. Nonetheless, both are well described by the scaling (S.4), yielding consistent estimates of  $\alpha_\infty^c$  and resulting in its smooth dependence on  $J$ , which can be seen on the phase diagrams shown in this work. For the entanglement  $S/S_P$ , however, the crossings are consistent with (S.4) for all considered values of  $J$ , as shown in Fig. S.2(b).

In all other extrapolations throughout this work, we also adopt Eq. (S.4).

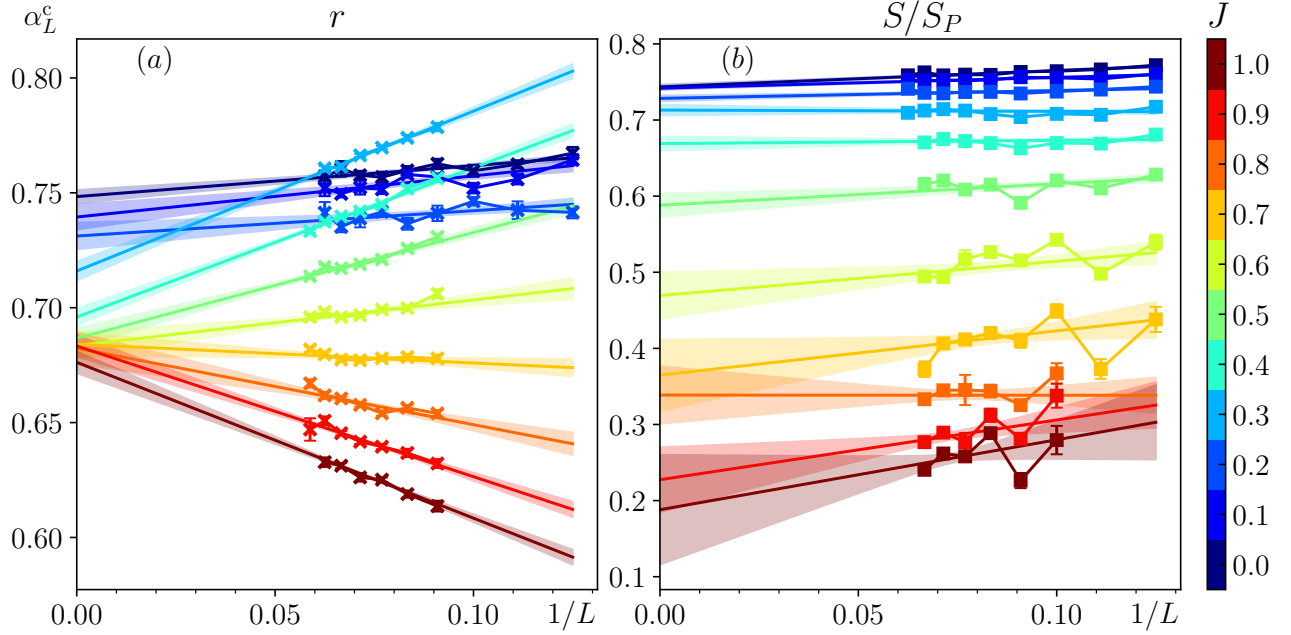


FIG. S.2. Extracted values of  $\alpha_L^c$  for the spectral gap ratio  $r$  and for rescaled half-chain entanglement entropies  $S/S_P$ . Colors correspond to values of  $J$ . Lines with shaded error band correspond to linear fits in  $1/L$ .